JOURNAL OF APPLIED ELECTROCHEMISTRY 26 (1996) 403–411

Anodic dissolution of rapidly quenched amorphous $Ni_{81}P_{19}$ alloys of different initial melt temperatures

L. PÉTER, G. LÁNG, L. KISS, J. SZALMA

Department of Physical Chemistry, Eötvös University, H-1518 Budapest 112, PO Box 32, Hungary

Received 25 April 1995; revised 25 August 1995

The anodic behaviour of rapidly quenched $Ni_{81}P_{19}$ samples prepared at different melt temperatures was investigated in 1.0 mol dm^{-3} aqueous HCl solution. The electrochemical properties of the alloys kept in melt at different temperatures are significantly influenced by the initial melt temperature. X-ray diffractometry suggests that this behaviour is associated with the presence of different quantities of crystalline secondary phase(s). On the basis of potentiodynamic polarization curves and potential–time functions recorded at constant current the alloys were characterized by a charge per surface unit amount proportional to the secondary phase content. A new model was proposed to characterize the anodic dissolution of alloys containing crystalline clusters.

1. Introduction

Nickel–phosphorus alloys are of great importance for corrosion protection, wear coating, electrical applications and catalysis. Several publications have dealt with the properties of Ni-P alloys and their surface layers produced by different methods [1–16]. Unfortunately, the results concerning the relationship between the properties and the preparation conditions are inconsistent. Experience has shown that corrosion behaviour of the alloy is also significantly influenced by its composition and, in the case of quenched alloys, by the temperature of the melt and the cooling rate.

The effects of the cooling rate on the corrosion properties of amorphous Ni–P alloys produced by rapid cooling were discussed in several papers [7, 8]. The corrosion rate of the samples increases with the sample thickness (i.e. with decreasing cooling rate).

Other investigations carried out on samples cooled from different initial melt temperatures have shown that the melt temperature has a significant influence on the electrochemical and corrosion properties of the samples before the formation of the passive surface layer [9, 10]. It seems, however, that there is no general agreement concerning the nature of this influence. According to certain authors [7, 8] the different electrochemical behaviour of the alloys is determined by the frequency of clusters having crystalline or alternative amorphous structure at the sample surface. On the other hand, some authors assumed that differences in the frequency of quenched-in defects and different relaxation states are responsible for the anodic behaviour of the alloys [15, 16]. Nevertheless, it is generally accepted that, after the formation of a phosphorus-rich passive layer, the corrosion process is determined mainly by the homogeneous structure of the covering layer [7, 15]. The presence of this phosphorus-rich layer have been proved by XPS [1, 12–15] but there are also indications by spectrophotometric analysis of P and Ni in the solution [8].

In this paper experimental results concerning the influence of the initial melt temperature on the anodic behaviour of rapidly quenched amorphous Ni–P alloys are reported. On the basis of a new model for the overall dissolution process, the origin of the differences observed in the polarization curves of the samples is explained.

2. Experimental details

The $Ni_{81}P_{19}$ alloy samples were produced by the quenching method. The melt of given composition was kept at the selected initial temperature for 20 min and was cooled with the help of a rotating copper cylinder of 0.35 m diameter at a rotation speed of 1750 min^{-1}. The initial melt temperatures are listed in Table 1.

Pieces of 0.10–0.25 cm^2 surface area were cut from the amorphous ribbons. The 'matt-side' of the samples (contacting with the cooling surface) was degreased by ethanol, polished manually with a no. 1000 SiC powder under ethanol, then washed and dried in air. A copper wire was attached to the other ('shiny') side of the sample with the help of a conducting adhesive and after drying it was attached to a suitable holder with an electrically insulating and chemically resistant inert silicon resin adhesive (registered trade mark 'F.BS', made by Materiál, Hungary). After the sticking operation the samples were kept in a desiccator filled with NaOH for at least 48 h to ensure reliable measurement. Rotating disc electrodes were prepared by fixing the polished sample to a Teflon holder as shown in Fig. 1. The holder was fixed to the rotating engine by a female screw.

All measurements were carried out in 1.0 M aqueous HCl solution at 22 ± 1 °C. Before immersing the sample into the solution oxygen was expelled from

0021-891X

Table 1. Sample numbering

Sample number	*Melt temperature/°C*
1	1600
2	1500
3	1400
4	1300
5	1100
6	1015

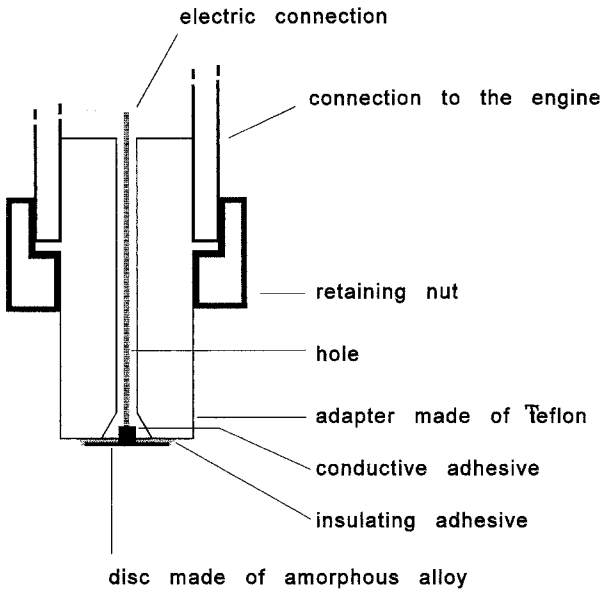

Fig. 1. Construction of the rotating disc electrode.

the whole measuring device and from the solution by high purity nitrogen.

The linear potential sweeps were started at −0.4 V vs SCE. Both the galvanostatic (potential decay) and potentiodynamic measurements on rotating disc

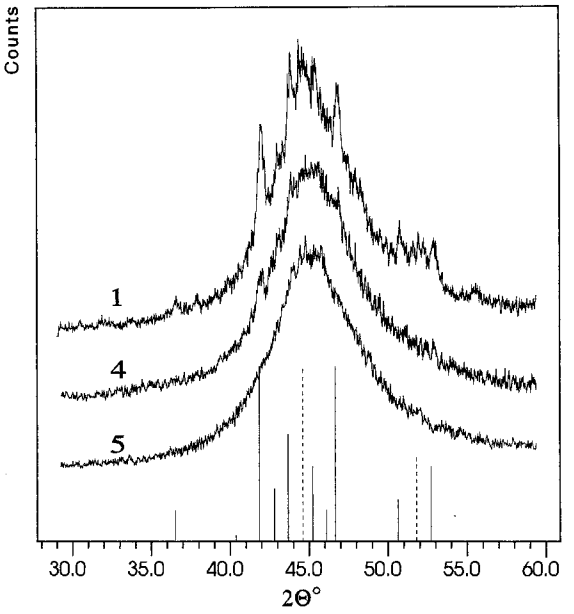

Fig. 2. The X-ray diffraction patterns measured for samples 1, 4 and 5. Other symbols: (solid lines) diffraction pattern of Ni; (dashed lines) diffraction pattern of Ni_3P.

electrodes were performed immediately after the electrode contacted the solution (within 30 s). The polarization curves for static electrodes were recorded 30 min after the sample was immersed into the electrolyte.

The usual three electrode system and a computer controlled potentiostat of type AFKEL 413/1 was used for the direct current measurements. The reported potentials refer to the saturated calomel reference electrode (SCE). The uncompensated solution resistance was compensated with resistance values computed from the impedance spectra (at the given cell design this value was usually 3.2 Ω). Impedance spectra were

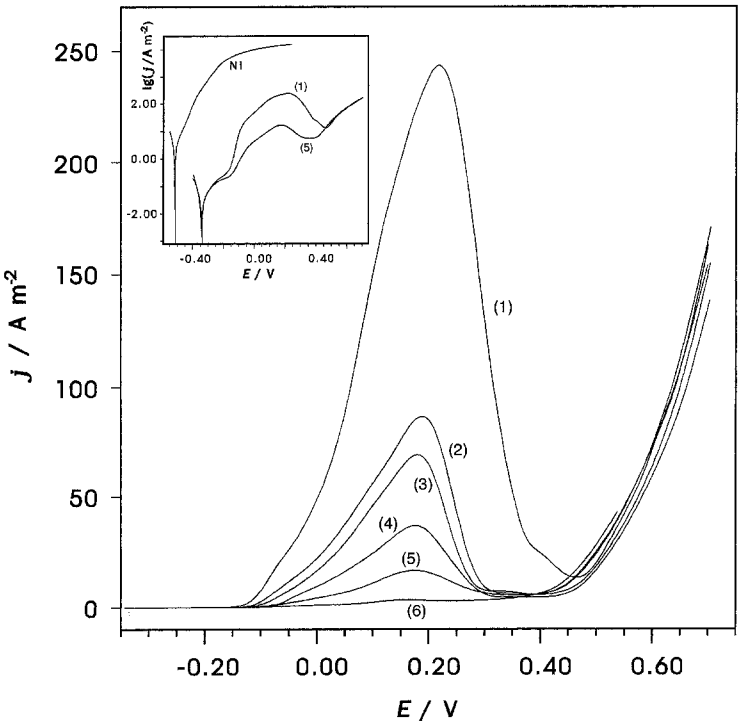

Fig. 3. Polarization curves for $Ni_{81}P_{19}$ samples measured at 10^{-3} V s^{-1} sweep rate on static electrodes in 1 M HCl. Curve numbers correspond to Table 1. Inset: Polarization curves of Ni and samples 1 and 5.

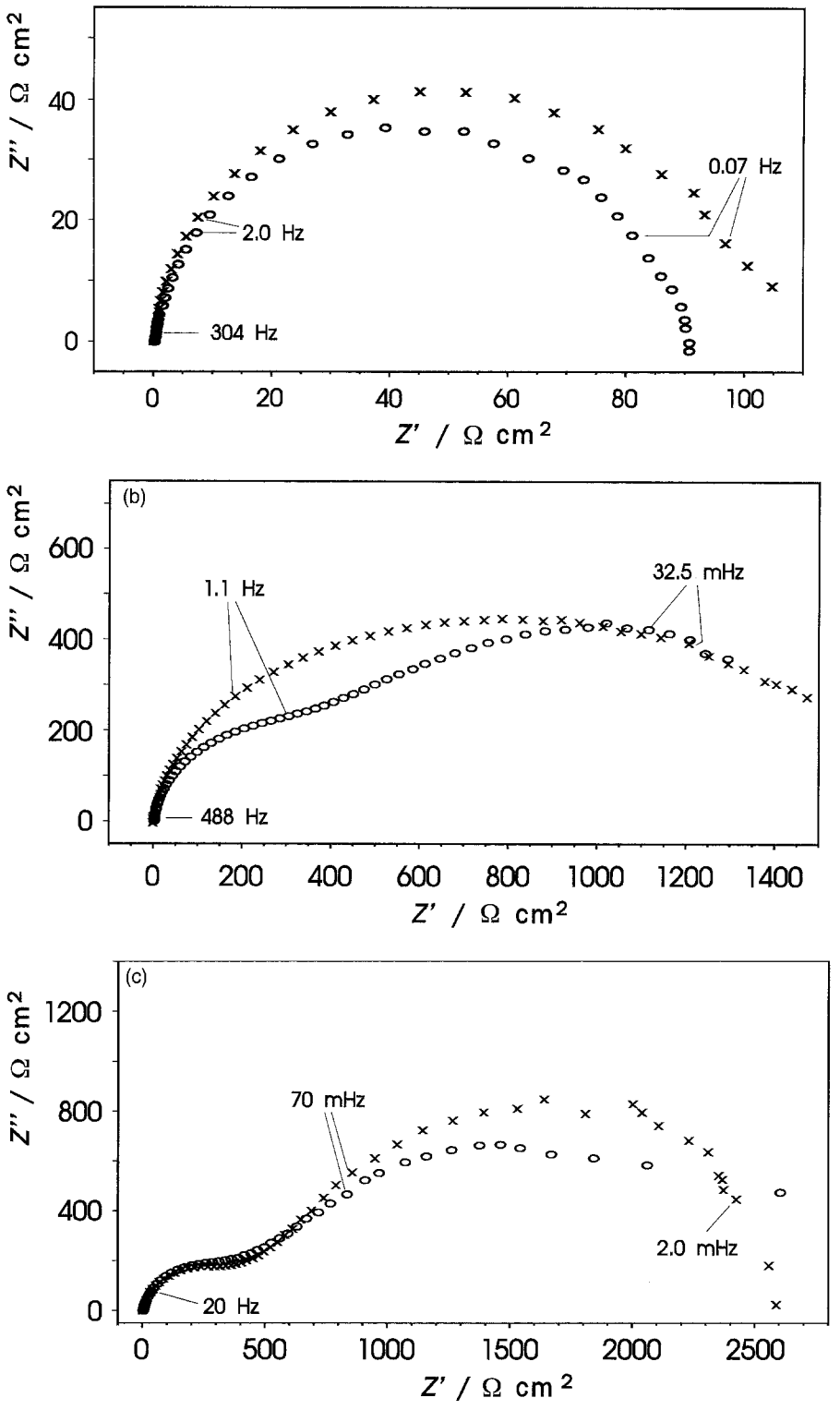

Fig. 4. Impedance spectra measured sequentially for the specimen 1 in 1 M HCl. (a) (O) first spectrum, (×) second spectrum; (b) (O) third spectrum (×) fourth spectrum; (c) (O) fifth spectrum, (×) sixth spectrum. Time of recording of individual curves: first and second spectra: 13 min, other spectra: 58 min.

recorded by computer controlled instruments (Solartron 1250 and Solartron 1286). The frequency of the impedance measurements ranged from 10 kHz to 5 mHz and a sinusoidal perturbation voltage of 5 mV peak to peak was used. A Siemens D 5000 type diffractometer was used for the X-ray measurements. The CuK_α radiation was generated at 40 kV and 30 mA.

3. Experimental results

X-ray diffractograms taken on samples 1, 4 and 5 are presented in Fig. 2. On the diffractogram of sample 1 well developed peaks indicating the presence of Ni and Ni_3P can be seen. The shape of the diffractogram of sample 5 is characteristic of a completely X-ray amorphous phase. Only very small amounts of crystalline phases seem to be present in sample 4.

Figure 3 shows the anodic sections of the polarization curves recorded on members of the sample series at 10^{-3} V s^{-1} polarization sweep rate. The height of the vertex in the anodic section of the curves changes monotonically with the melt temperature measured before quenching. The potentiostatic polarization curves were practically identical for all samples, in good agreement with the results of Habazaki *et al.* [15].

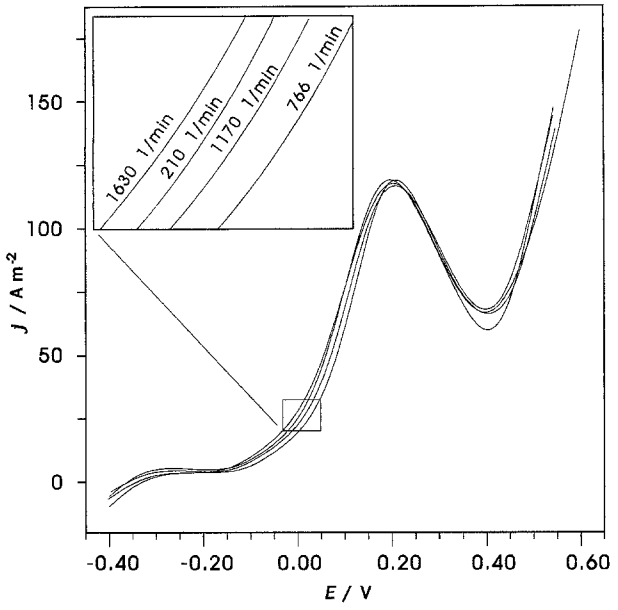

Fig. 5. First (initial) polarization curves recorded at different disc rotation speeds for sample 2 in 1 M HCl. Polarization sweep rate: 10^{-3} V s^{-1}.

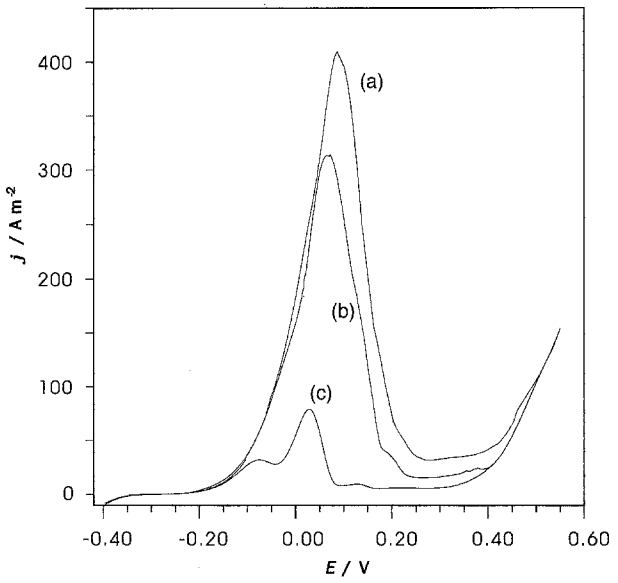

Fig. 6. First polarization curves measured on sample 1 by potentiodynamic method in 1 M HCl. Polarization sweep rates: (a) 3.67×10^{-4}, (b) 2.10×10^{-4} and (c) 1.15×10^{-4} V s^{-1}.

Impedance spectra were recorded subsequently (one scan after the other) on the sample 1 at 0.010 V vs SCE. This potential was selected to correspond to the ascending line of the polarization curve and also to avoid too high dissolution rates. The corresponding spectra are shown in Fig. 4.

The curves indicate that the polarization resistance of the dissolving sample increases with time, and diffusion may be important in the overall process. To clarify the role of diffusion in the anodic dissolution of the samples rotating disc electrodes were prepared from them.

Polarization curves recorded on sample 2 at different rotation speeds and at 10^{-3} V s^{-1} sweep rate are plotted in Fig. 5. It can be clearly seen that the dependence of the rate of dissolution on the

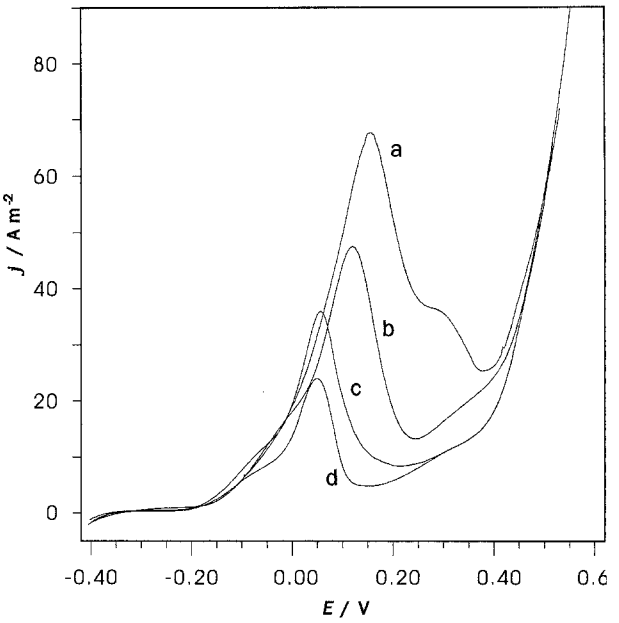

Fig. 7. First polarization curves measured on sample 4 by potentiodynamic method in 1 M HCl. Polarization sweep rates: (a) 9.50×10^{-4}, (b) 5.58×10^{-4}, (c) 2.23×10^{-4} and (d) 1.33×10^{-4} V s^{-1}.

rotation speed is not significant, therefore further measurements were made at 1170 rpm only.

First ('initial') polarization curves recorded at various polarization sweep rates are shown in Fig. 6 for sample 1 and in Fig. 7 for sample 4, respectively. The series of curves referring to samples of identical quality indicate that the height of the peak depends on the polarization rate. The peak height is proportional to the polarization sweep rate. At very low sweep rate (10^{-4} V s^{-1} or lower) the potentiodynamic polarization curve approaches the curve which can be recorded by the potentiostatic method. A similar phenomenon is, of course, well known from the theory of cyclic voltammetry. The scale of changes in the shape of the curves here, however, in comparison with the applied slow polarization rates, seems to be too great as to be interpreted by the effects taken into account in the above mentioned theory.

Anodic polarization curves recorded subsequently using a simple specimen showed the same behaviour as reported in [7]. The shape of the curves changed on repeated recording, but after 3–8 anodic sweeps (depending on the sweep rate) the subsequent curves were practically identical. This behaviour can be easily explained by the formation of a well-defined covering layer [7, 15].

Potential–time functions recorded at constant current densities are plotted in Fig. 8 for sample 1 and in Fig. 9 for sample 4. At the start of the polarization the potential changes suddenly from the corrosion potential to an anodic one, followed by a smaller minimum and the potential becomes steady after a relatively rapid change in the positive direction. The charge passing through the sample surface required to reach the steady potential is about 10 times less in the case of sample 4 than in the case of sample 1.

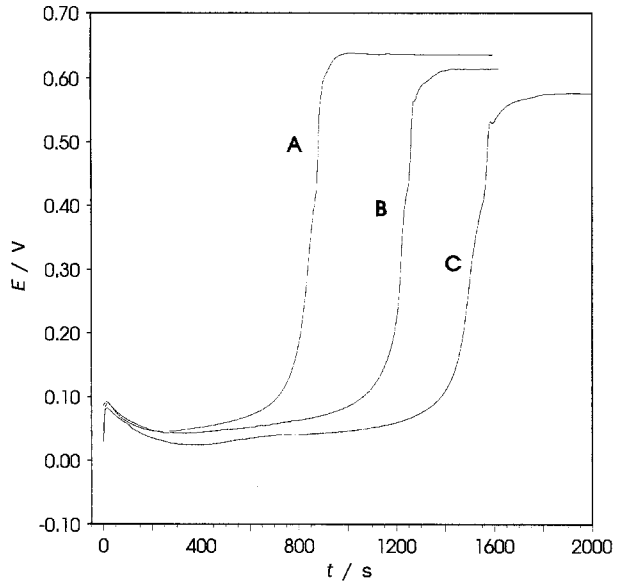

Fig. 8. Potential against time curves measured on sample 1 in 1 M HCl. Current densities: (a) 208.6, (b) 148.7 and (c) 111.1 A m^{-2}.

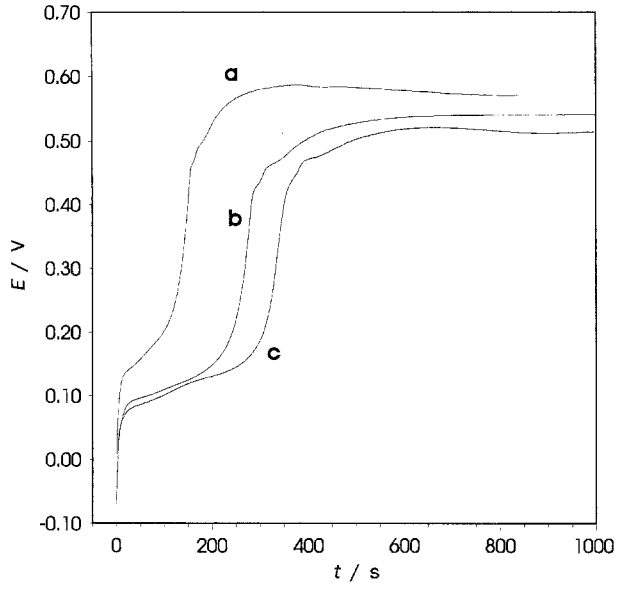

Fig. 9. Potential against time curves measured on sample 4 in 1 M HCl. Current densities: (a) 89.24, (b) 51.45 and (c) 39.22 A m^{-2}.

4. Discussion

The electrochemical behaviour of a given sample immediately after immersion into the solution is determined by the properties of the polished surface. It is obvious that the properties (i.e., the structure and the composition) of the clean surface are very similar to those of the bulk. Therefore, the variation in the first (initial) polarization curves can be attributed to the structural differences in the bulk of the samples. After the formation of the phosphorus-rich surface layer the dissolution process is governed by the structure of this film [7, 15].

The X-ray diffractograms show that some members of the sample series contain crystalline phases. Earlier results of Mössbauer spectroscopy indicate that even samples found completely amorphous by X-ray diffractometry may contain clusters or centres of alternative structure or dissimilar composition [9, 10]. Comparing the diffractograms and the anodic section of the potentiodynamic polarization curves it is obvious that the height of the peaks is related to the amounts of the crystalline phases in the samples (Fig. 2 and Fig. 3).

The assumption that the presence of crystalline phases causes an increase in anodic current density relative to the completely amorphous alloys is in good agreement with earlier results [17]. It was demonstrated in [17] that the oxidation of phosphinate anion on the surface of amorphous Ni–P alloys is considerably more hindered than on crystalline alloys. Therefore, the absorbed phosphinate acts as a protective layer on the amorphous Ni–P surface in the potential region in which the anodic oxidation and dissolution of crystalline components take place at a relatively high rate [17].

On the basis of this observation the following model can be proposed to explain the differences in the anodic behaviour of the alloys. It may be supposed that the rate constants of dissolution of the clusters or domains of the secondary phases are much higher than the same constant characterising the bulk matrix, which is partially covered with the phosphorus-rich surface layer. At the surface of the clusters contacting the solution the dissolution rate is high and therefore a phosphorus-rich layer cannot be formed. After the dissolution of the secondary phase clusters the measured current returns to the value characteristic of the dissolving matrix. In this case the peaks on the polarization curves may be explained by the dissolution of the clusters. The change of the surface state is demonstrated in Fig. 10.

On the other hand, at measurements with constant current the accomplishment of the dissolution of secondary phase(s) is associated with the appearance of a rapid positive potential change in the potential against time function.

When the surface of the sample is completely covered with the phosphorus-rich layer the peak corresponding to the secondary phase clusters does

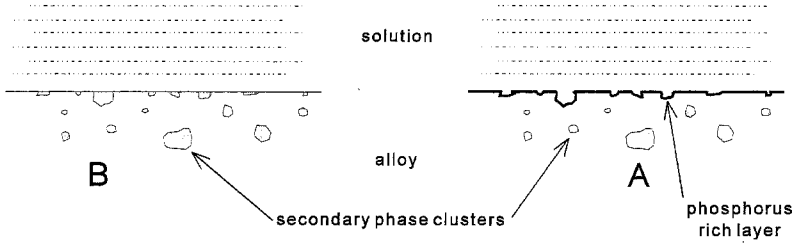

Fig. 10. State of the sample surface before (B) and after (A) the dissolution of the secondary phase clusters close to the surface.

not appear on the polarization curve. The phosphorus-rich covering layer may slowly thicken even after the exhaustion of clusters of secondary phases contacting the solution.

For the construction of a simple kinetic model reflecting the sample behaviour during the first anodic sweep we assume that before anodic polarization ($t = 0$, where t is the time) a small Θ_0 fraction of the sample surface is covered with the secondary phase. At time t after starting the anodic polarization the coverage is $\Theta(t)$.

The current density is the sum of the anodic current densities originating from the dissolution of the secondary phase and the matrix:

$$j_t = k_c\Theta \exp(b_c E) + k_m[1 - \Theta] \exp(b_m E) \qquad (1a)$$

and

$$j_t = j_c + j_m \qquad (1b)$$

where b_c and b_m are the reciprocal Tafel constants characteristic of the anodic dissolution of the secondary phase and the matrix, respectively. E is the electrode potential referring to a given reference electrode; k_c and k_m are the corresponding rate constants (independent from the electrode potential); j_c and j_m are the current densities rising from the secondary phase and the matrix, respectively; j_t is the total current density. The rate constant k_m characterizing the dissolution of the matrix is regarded as unrelated to the change proceeding in the sample surface. This can be accepted if we assume that the matrix surface is enriched in phosphorus at the start and the change in the value of k_m with thickening of the layer is quite small. For mathematical simplicity it is also assumed that the $j_m = k_m[1 - \Theta] \exp(b_m E)$ expression describes the dissolution of the metal and the oxidation of the metalloid simultaneously.

Assuming now that $k_c \gg k_m$ and applying the approach $j_m \approx k_m \exp(b_m E)$ for the total current density we get (Θ is very small):

$$j_t = k_c\Theta \exp(b_c E) + k_m \exp(b_m E) \qquad (2)$$

With the assumption that the change of the coverage of the surface with clusters $\Theta(t) - \Theta_0$ is proportional to the charge expended on the dissolution of clusters:

$$\Theta(t) = \Theta_0 - \frac{1}{\varphi} Q(t) = \Theta_0 - \frac{1}{\varphi} \int_0^t j_c \, dt \qquad (3)$$

where φ is a proportionality factor, $Q(t)$ is the charge passing through surface unit during time t on account of dissolving secondary phase. The electrode potential is a linear function of time:

$$E(t) = E_0 + vt \qquad (4)$$

where v is the sweep rate and E_0 is the starting potential. From Equations 2, 3 and 4,

$$j_c = k_c\Theta_0 \exp(b_c E) - \frac{k_c}{v\varphi} \exp(b_c E) \int_{E_0}^{E} j_c \, dE \qquad (5)$$

After multiplying both sides of Equation 5 with $\exp(-b_c E)$ and differentiating with respect to E,

$$\frac{dj_c}{dE} \exp(-b_c E) + j_c \left[\frac{k_c}{v\varphi} - b_c \exp(-b_c E)\right] = 0 \qquad (6)$$

The differential Equation 6 can be solved taking into account the boundary condition $j_c(t = 0) = k_c\Theta_0 \exp(b_c E_0)$:

$$j_c = k_c\Theta_0 \exp\left[\frac{k_c}{v\varphi b_c} \exp(b_c E_0)\right] \times \exp\left[b_c E - \frac{k_c}{v\varphi b_c} \exp(b_c E)\right] \qquad (7)$$

After substituting Equation 7 into Equation 2 the total current density is

$$j_t = k_m \exp(b_m E) + k_c\Theta_0 \exp\left[\frac{k_c}{v\varphi b_c} \exp(b_c E_0)\right] \times \exp\left[b_c E - \frac{k_c}{v\varphi b_c} \exp(b_c E)\right] \qquad (8a)$$

If we supplement Equation 8a with a term related to the cathodic process (reduction of depolarizer) we obtain:

$$j_t = -k_k c_D \exp(-b_k E) + k_m \exp(b_m E) + k_c\Theta_0 \times \exp\left[\frac{k_c}{v\varphi b_c} \exp(b_c E_0)\right] \exp\left[b_c E - \frac{k_c}{v\varphi b_c} \exp(b_c E)\right] \qquad (8b)$$

where c_D is the concentration of the depolarizer, b_k is the reciprocal Tafel constant and k_k is the rate constant of the depolarizer reduction.

(It should be mentioned that Equation 7 is formally equivalent to the expression derived in [18] for totally irreversible reactions in a thin layer cell).

The character of some polarization curves and the X-ray diffractograms suggest that there are several types of secondary phase. This is indicated by the inflections in the potential against time functions (Figs 8 and 9) and also the plateaux superposed on the peaks in some of the polarization curves (Figs 6 and 7). These observations correspond to the results of Crousier *et al.* [6] for electrochemically deposited Ni–P alloys. In the presence of several secondary phases the number of the parameters to be taken into account increases, since the secondary phase i exhibits k_i, $\Theta_{0,i}$, and φ_i values. If each Θ_i is the function of the charge passed through the surface during the anodic dissolution of secondary phase i and does not depend on the coverage of the surface with the other secondary phases, the equation of the polarization curve implies the sum of the expressions characteristic of the secondary phases:

$$j_t = -k_k c_D \exp(-b_k E) + k_m \exp(b_m E) + \sum_{i=1}^{N} k_{c,i}\Theta_{0,i} \exp\left[\frac{k_{c,i}}{v\varphi_i b_{c,i}} \exp(b_{c,i} E_0)\right] \times \exp\left[b_{c,i} E - \frac{k_{c,i}}{v\varphi_i b_{c,i}} \exp(b_{c,i} E)\right] \qquad (9)$$

where N is the number of the secondary phases.

Several attempts were made to estimate the parameters in Equation 8b by the nonlinear least squares fitting method. Unfortunately the mathematical structure of Equation 8b does not allow the determination of each parameter even in the presence of one secondary phase only. Equation 8b can be transformed as follows:

$$j_t = -p_1 \exp(-p_2 E) + p_3 \exp(p_4 E) + p_5 \exp[p_6 E - p_7 \exp(p_6 E)] \quad (10)$$

where $p_1 = k_k c_D$, $p_2 = b_k$, $p_3 = k_m$, $p_4 = b_m$, $p_5 = k_c \Theta_0 \exp[(k_c/v\varphi b_c)\exp(b_c E_0)]$, $p_6 = b_c$, $p_7 = (k_c/v\varphi b_c)$. Equation 8b contains 11 parameters, but in Equation 10 only seven parameters can be regarded as independent and one parameter (Θ_0, k_c or φ) should be known from independent measurement for a reliable parameter estimation since c_D, E_0 and v are determined by the measurement conditions.

Besides the above mentioned mathematical difficulties, the neglect of terms in the evaluation of the polarization curve equation results in parameter estimation that is not completely reliable:

(a) The proposed model is not suitable for the delineation of polarization curves recorded by potentiodynamic method at very low polarization sweep rates ($v < 10^{-4}\,V\,s^{-1}$). The surface area covered with secondary phase may significantly change due to spontaneous corrosion and not only as a result of anodic dissolution. This might be the reason for the considerably lower peak current densities in the polarization curves in Fig. 3 compared to the curves which were taken immediately after the immersion of the sample into the solution.

(b) Galvanostatic curves in Fig. 8 indicate another phenomenon not taken into consideration. After the start of the dissolution the real surface area of the samples increases, mainly as a result of roughening of the surface of secondary phase clusters contacting the solution. The above model considers neither the increase in the real surface area of the sample nor the effect of the increasing thickness of the surface layer.

Nevertheless the model reflects the electrochemical properties of the alloys tested as can be seen from the computer simulations of the polarization curves. In Figs 11 and 12 simulated polarization curves were obtained using Equation 8b. Some of the simulation parameters used (k_m, b_m, k_k, b_k) were obtained on the basis of the best fit of the measured polarization curves in the anodic and cathodic potential regions far from the anodic current peak. The other parameters were varied manually until the simulated polarization curves approximated the shape of the curves.

If can be seen that using realistic simulation parameters the area under the peak is proportional to the charge required for the dissolution of the secondary phase and, after the dissolution of the secondary phase, the anodic sections of the curves coincide. Polarization curves calculated on the basis of Equation 10 using several different N values are demonstrated in Fig. 13.

The impedance spectra are characteristic of coupled charge transfer and diffusion processes. The diffusion section is probably the consequence of nickel ion diffusion through the phosphorus-rich layer. This is confirmed by the curves in Fig. 5, namely, if the diffusion sections of the impedance spectra is caused

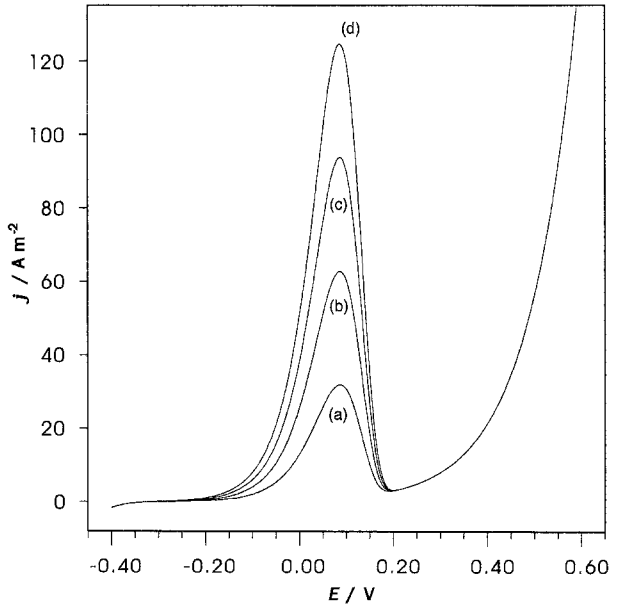

Fig. 11. Polarization curves simulated on the basis of Equation 8b. Data used for simulation are: $b_k = 31.25\,V^{-1}$, $b_m = 9.71\,V^{-1}$, $b_c = 20\,V^{-1}$, $E_0 = -0.4\,V$, $c_D = 1\,mol\,dm^{-3}$, $k_c = 1500\,A\,m^{-2}$, $k_m = 0.44\,A\,m^{-2}$, $k_k = 6.14 \times 10^{-6}\,A\,m^{-2}\,mol^{-1}\,dm^3$, $\varphi = 7 \times 10^5$ $C\,m^{-2}$, $v = 6 \times 10^{-4}\,V\,s^{-1}$. Θ_0 for different curves: (a) 0.01, (b) 0.02, (c) 0.03 and (d) 0.04.

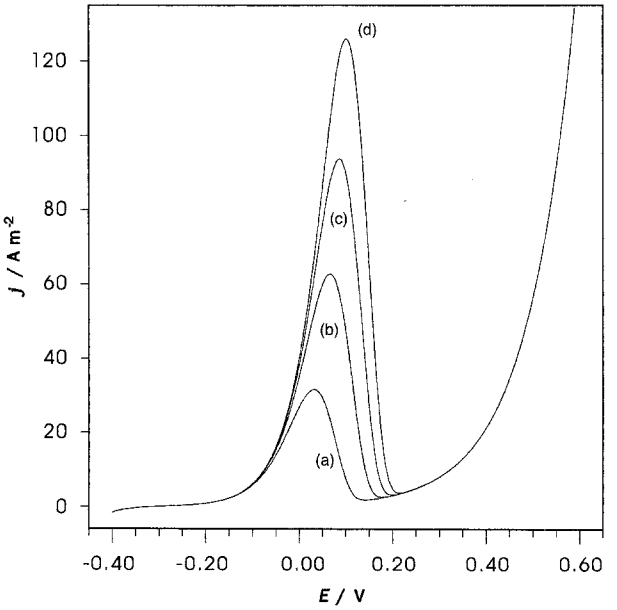

Fig. 12. Polarization curves simulated on the basis of Equation 8b. Data used for simulation: $b_k = 31.25\,v^{-1}$, $b_m = 9.71\,V^{-1}$, $b_c = 20\,V^{-1}$, $\Theta_0 = 0.03$, $E_0 = -0.4\,V$, $c_D = 1\,mol\,dm^{-3}$, $k_m = 0.44$ $A\,m^{-2}$, $k_k = 6.14 \times 10^{-6}\,A\,m^{-2}\,mol^{-1}\,dm^3$, $\varphi = 7 \times 10^5\,C\,m^{-2}$, $k_c = 1500\,A\,m^{-2}$. The sweep rate v for individual curves: (a) 2×10^{-4}, (b) 4×10^{-4}, (c) 6×10^{-4} and (d) $8 \times 10^{-4}\,V\,s^{-1}$.

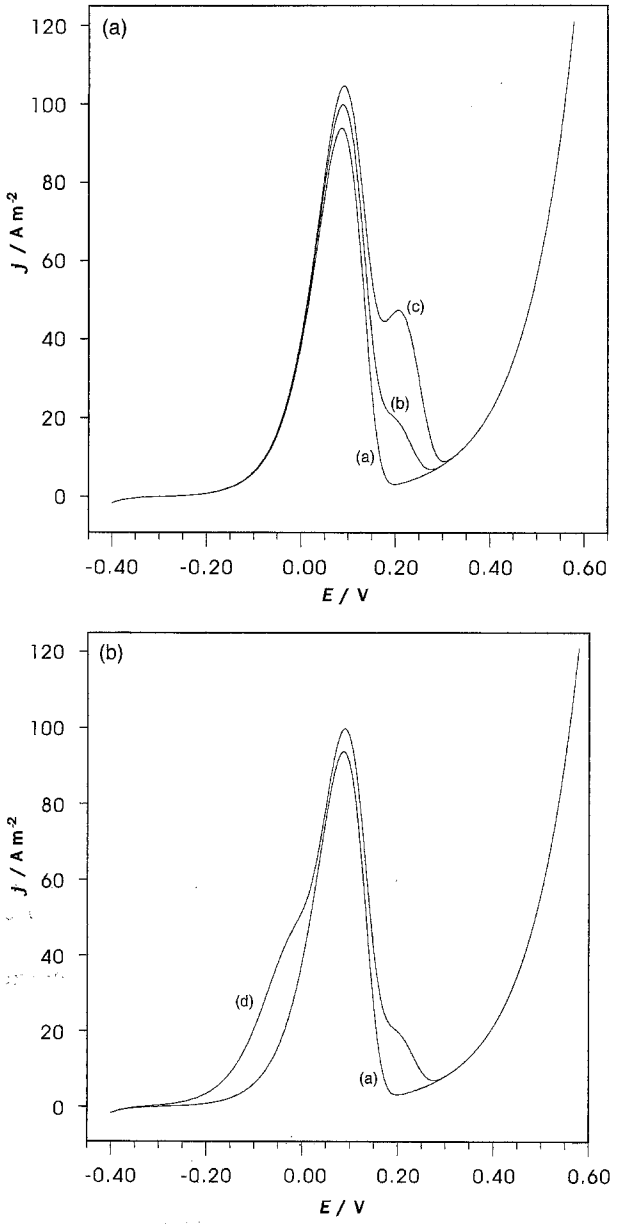

Fig. 13. Polarization curves simulated on the basis of Equation 9 for $N = 2$ and $N = 3$. Data used for simulation: $b_k = 31.25\,V^{-1}$, $b_m = 9.71\,V^{-1}$, $b_{c,1} = 20\,V^{-1}$, $\Theta_{0.1} = 0.03$, $E_0 = -0.4\,V$, $c_D = 1\,mol\,dm^{-3}$, $k_m = 0.44\,A\,m^{-2}$, $\varphi_1 = 7 \times 10^5\,C\,m^{-2}$, $k_k = 6.14 \times 10^{-6}\,A\,m^{-2}\,mol^{-1}\,dm^3$, $k_{c,1} = 1.5 \times 10^3\,A\,m^{-2}$, $v = 6 \times 10^{-4}\,V\,s^{-1}$. (Curve (a) is identical to curve (c) of Fig 11 and curve (c) of Fig. 12). Other data for individual curves: (b) $b_{c,2} = 20\,V^{-1}$, $\Theta_{0.2} = 0.01$, $\varphi_2 = 4 \times 10^5\,C\,m^{-2}$, $k_{c,2} = 120\,A\,m^{-2}$; (c) $b_{c,2} = 20\,V^{-1}$, $\Theta_{0.2} = 0.025$, $\varphi_2 = 4 \times 10^5\,C\,m^{-2}$, $k_{c,2} = 80\,A\,m^{-2}$; (d) $b_{c,2} = 20\,V^{-1}$, $b_{c,3} = 20\,V^{-1}$, $\Theta_{0.2} = 0.01$, $\Theta_{0.3} = 0.01$, $\varphi_2 = 4 \times 10^5\,C\,m^{-2}$, $\varphi_3 = 5 \times 10^5\,C\,m^{-2}$, $k_{c,2} = 120\,A\,m^{-2}$, $k_{c,3} = 1.5 \times 10^4\,A\,m^{-2}$.

by diffusion of the components in the solution, the polarization curves would be dependent on the electrode rotation speed. The increase in the charge transfer resistance may be related mainly to decrease in the area covered by secondary phase while the diffusion sections may be related ot the thickening of the phosphorus-rich surface layer. The nature of the sample surface is continuously changing during dissolution as a consequence of both secondary phase dissolution described by the model and the formation of a phosphorus-rich layer. Therefore, the polarization resistance of the samples increases with time.

Table 2. Calculated charge related to the dissolution of crystalline clusters for sample 1

Basis	$v/V\,s^{-1}$	*Charge per unit geometrical surface* $/C\,m^{-2}$
Polarization curves	1.15×10^{-4}	7.80×10^4
	2.10×10^{-4}	2.21×10^5
	3.67×10^{-4}	1.63×10^5
	$j/A\,m^{-2}$	
Galvanostatic curves	111.1	1.77×10^5
	148.7	1.90×10^5
	208.6	1.89×10^5

Table 3. Calculated charge related to the dissolution of crystalline clusters for sample 4

Basis	$v/V\,s^{-1}$	*Charge per unit geometrical surface* $/C\,m^{-2}$
Polarization curves	1.33×10^{-4}	1.69×10^4
	2.23×10^{-4}	2.10×10^4
	5.58×10^{-4}	1.19×10^4
	9.5×10^{-4}	1.05×10^4
	$j/A\,m^{-2}$	
Galvanostatic curves	39.22	1.66×10^4
	51.45	1.57×10^4
	89.24	1.59×10^4

The differences between the dissolution properties of the alloys were characterized by a charge per unit surface. Supposing that the dissolution of the amorphous matrix is not considerable while the secondary phase clusters completely dissolve, this quantity is characteristic of the amount of the secondary phase clusters (positioned in the vicinity of the surface). Using the results of the potentiodynamic and galvanostatic experiments two different methods were applied for this calculation:

(a) The areas under the peaks of the potentiodynamic polarization curves were calculated by numerical integration and the values obtained were divided by the corresponding polarization rates.
(b) The times required for reaching steady state (read-off the potential against time curves) were multiplied by the corresponding current densities.

The results are presented in Tables 2 and 3.

The data in Tables 2 and 3 show that significant quantities of secondary phases are present in some specimens. This observation is in very good agreement with the results of the X-ray diffractometric measurements showing the presence of well detectable amounts of crystalline Ni and Ni_3P in sample 1 and only a very small quantity of crystalline phase in sample 4.

Recent results imply that the explanation proposed in some earlier works [9, 15, 16] for describing the

difference in the anodic current densities during anodic polarization are questionable. The assumption that quenched-in defects are responsible for the increased anodic current density is probably insufficient. In [15, 16], the behaviour of the annealed specimen is reported as a result of structural relaxation during the stabilization at 340 °C. This explanation is satisfactory if the anodic polarization curves of the samples prepared by rapid quenching of the white heat melt and the annealed sample are compared. Comparing the anodic polarization curves of the annealed sample and the sample prepared from the red heat melt the increased anodic current density cannot be the result of a relaxation process only. The change in the electrochemical behaviour due to the 'stabilization' may also be the result of partial crystallisation. Although the X-ray diffractograms of quenched ribbons [15] do not show considerable differences, besides the structural relaxation the influence of partial crystallisation cannot be automatically excluded.

5. Conclusions

Present results support the earlier finding that the electrochemical properties of rapidly quenched $Ni_{81}P_{19}$ alloys are strongly influenced by the preparation parameters. Samples of the same composition kept in melt at different temperatures before rapid cooling may exhibit drastically different corrosion properties. The proposed kinetic model suggests that the main cause of the change in behaviour is the different crystalline phase content of the amorphous matrix. The nonhomogeneous structure of the amorphous samples results in decreased corrosion resistance. However, alloys with excellent corrosion properties can be obtained by using optimized fabrication parameters. Earlier experiments [7, 8] showed that electrochemical properties are closely related to the cooling rate. According to recent results the most favourable initial melt temperature is close to the eutectic temperature of the system. The above observations may be very important for industrial applications, since rapidly quenched amorphous alloys of excellent corrosion properties can only be made by using optimal preparation conditions. On the other hand, the proposed kinetic model allows the characterization of amorphous NiP alloys prepared at different conditions even if only very small structural differences can be detected by diffraction techniques.

Acknowledgements

Financial support from the National Research Fund (OTKA-F4190 and OTKA-2113) are gratefully acknowledged. The X-ray diffractograms were measured in the laboratory of the Department of Mineralogy of the Eötvös University with the help of Dr G. Lovas. The authors also thank I. Molnár for his technical assistance.PP

References

[1] A. Kawashima, K. Asami and K. Hashimoto, *Corr. Sci.* **24** (1984) 807.
[2] A. Królikowski, M. Pelowska and P. Butkiewicz, *Metallurgy and Foundry Engng* **18** (1992) 189.
[3] E. Bredael, B. Blanpain, J. P. Celis and J. R. Roos, *J. Electrochem. Soc.* **141** (1994) 294.
[4] A. Królikowski and P. Butkiewicz, *Electrochim. Acta* **38** (1993) 1979.
[5] R. Zeller and U. Landau, *J. Electrochem. Soc.* **139** (1992) 3464.
[6] J. Crousier, Z. Hanane and J.-P. Crousier, *Electrochim. Acta* **38** (1993) 261.
[7] Gy. Láng, L. Kiss, L. A. Ivanov, S. A. Sokolov, I. A. Novochatski and L. Földi, *Acta Chim. Hung.* **128** (1991) 807.
[8] L. A. Janov, S. A. Sokolov, J. A. Novochatski, Gy. Láng and L. Kiss, *Acta Chim. Hung.* **129** (1992) 605.
[9] E. Kuzmann, A. Pákozdi, A. Vértes, Gy. Láng, L. Kiss, J. Ensling, I. A. Novochatski and L. A. Ivanov, *J. Radioanal. Nucl. Chem.* **146** (1990) 159.
[10] A. Cserei, E. Kuzmann, F. Hajdú, L. Pöppl, Gy. Láng, A. Vértes, L. Kiss, I. A. Novochatski and I. A. Usatyuk, *ACH – Models in Chemistry* **29** (1992) 469.
[11] A. Kawashima, K. Asami and K. Hashimoto, *Corros. Sci.* **25** (1985) 1103.
[12] R. B. Diegle, N. R. Sorensen and G. C. Nelson, *J. Electrochem. Soc.* **33** (1986) 1769.
[13] R. B. Diegle, C. R. Clayton, Y. Lu and N. R. Sorensen, *J. Electrochem. Soc.* **34** (1987) 138.
[14] R. B. Diegle, N. R. Sorensen, C. R. Clayton, M. A. Helfand and Y. C. Yu, *J. Electrochem. Soc.* **135** (1988) 1085.
[15] H. Habazaki, S. Q. Ding, A. Kawashima, K. Asami, K. Hashimoto, A. Inoue and T. Masumoto, *Corros. Sci.* **29** (1989) 1319.
[16] H. Habazaki, Y.-P. Lu, A. Kawashima and K. Hashimoto, *Corros. Sci.* **32** (1991) 1227.
[17] U. Hoffman and K. G. Weil, *Corros. Sci.* **34** (1993) 423.
[18] A. Y. Hubbard and F. C. Anson, '*Electroanalytical Chemistry*', Vol. 4 (edited by A. J. Bard), Marcel Dekker, New York (1970) p. 129.